Inorg. Chem. **2006**, *45*, 883–893

Synthesis and Crystal and Electronic Structures of the $Na_2(Sc_4Nb_2)(Nb_6O_{12})_3$ Octahedral Niobium Cluster Oxide. Structural Correlations between $A_nBM_6L_{12}(Z)$ Series and Chevrel Phases

Stéphane Cordier,* Kaplan Kirakci, Bruno Fontaine, Jean-François Halet, Régis Gautier, and Christiane Perrin

Laboratoire de Chimie du Solide et Inorganique Moléculaire, UMR 6511 CNRS-Université de Rennes 1, ENSC Rennes, Institut de Chimie de Rennes, Avenue du Général Leclerc, F-35042 Rennes Cedex, France

Received July 28, 2005

We report here the synthesis and crystal and electronic structures of the $Na_2(Sc_4Nb_2)(Nb_6O_{12})_3$ niobium oxide whose structure is related to that of $Ti_2Nb_6O_{12}$. It constitutes a new member of the larger $A_nBM_6L_{12}(Z)$ families (A = monovalent cation located in tetrahedral cavities of units, B = monovalent or trivalent cations located in octahedral cavities of units, M = rare earth, Zr, or Nb, Z = interstitial except for M = Nb). The structural relationships between the $A_nBM_6L_{12}(Z)$ series ($M_6L^i_{12}L^a_6$ unit-based compounds with a $M_6L^i_6L^{i-a}_{6/2}L^{a-i}_{6/2}$ cluster framework) and Chevrel Phases ($M_6L^i_8L^a_6$ unit-based compounds with a $M_6L^i_2L^{i-a}_{6/2}L^{a-i}_{6/2}$ cluster framework) are shown in terms of M_6L_{18} and M_6L_{14} unit packing. Despite a topology similar to that encountered in Chevrel Phases, intercalation properties are not expected in the $Nb_6O^i_6O^{i-a}_{6/2}O^{a-i}_{6/2}$ cluster framework-based compounds. Finally, it is shown, from theoretical LMTO calculations, that a semiconducting behavior is expected for a maximum VEC of 14 in the $Nb_6O^i_6O^{i-a}_{6/2}O^{a-i}_{6/2}$ cluster framework.

Introduction

Metallic octahedral clusters are characterized by metal−metal bond lengths close to those found in the corresponding metals. They are formed via solid state synthesis with early transition metal elements in their low oxidation states.[1,2] The $[(M_6L^i_{12})L^a_6]^{n-}$ (L = F, Cl, Br, O) and $[(M_6L^i_8)L^a_6]$ (L = Cl, Br, I, S, Se, Te) units (a = apical and i = inner, according to the Schäfer and Schnering notation[3]) constitute the basic building blocks in the solid-state octahedral cluster chemistry. These octahedral clusters are bonded to six terminal ligands (L^a) in both types of unit, but they are either edge-bridged by twelve inner ligands (L^i) in the $[(M_6L^i_{12})L^a_6]^{n-}$ entity or face-capped by eight inner ligands (L^i) in the $[(M_6L^i_8)L^a_6]$ unit.[4] The physical properties of these cluster compounds are related to the strength of the interaction between cluster units and to the number of electrons available for metal−metal bonding within the cluster, the so-called valence electron count (VEC). The molecular orbital (MO) diagrams show a set of eight metal−metal bonding molecular orbitals (a_{1g}, t_{1u}, t_{2g}, and a_{2u} in O_h symmetry) for the $M_6L^i_{12}L^a_6$ unit and a set of twelve metal−metal bonding molecular orbitals (a_{1g}, t_{1u}, t_{2g}, t_{2u}, and e_g in O_h symmetry) for the $M_6L^i_8L^a_6$ unit. Consequently, their full occupation leads to a closed-shell configuration with a VEC of 16 for the former[5] and a VEC of 24 for the latter.

Transition metal halides and chalcohalides based on discrete $M_6L^i_8X^a_6$ (M = Mo, Re, W; L = halogen or chalcogen, X = halogen) units or X^{a-a} interconnected units, ($M_6L^i_8X^{a-a}_{x/2}X^a_{6-x}$ (x = 2, 4, 6)) exhibit a strong molecular character characterized by a VEC of 24 e^-/M_6 and insulating properties. On the other hand, the progressive condensation of $M_6L^i_8L^a_6$ units via L^{i-a}/L^{a-i} chalcogen ligands in one,[6] two,[7] and three directions[8] (1-, 2-, 3D) engenders stronger

* To whom correspondence should be addressed. Email: stephane.cordier@univ-rennes1.fr. Fax: +33 2 23 23 67 99.

(1) Simon, A. *Angew. Chem., Int. Ed.* **1988**, *27*, 159.
(2) Braunstein, P.; Oro, L. A.; Raithby P. R. *Metal Clusters in Chemistry*, Vol. II.; Wiley-VCH: Weinheim, Germany, 1999.
(3) Schäfer, H.; von Schnering, H. G. *Angew. Chem.* **1964**, *76*, 833.
(4) Perrin, C. *J. Alloys Compd.* **1997**, *262*−*263*, 10.
(5) Ogliaro, F.; Cordier, S.; Halet, J.-F.; Perrin, C.; Saillard, J.-Y.; Sergent, M. *Inorg. Chem.* **1998**, *37*, 6199.
(6) Perrin, C.; Potel, M.; Sergent, M. *Acta Crystallogr.* **1983**, *C39*, 415.
(7) Leduc, L.; Perrin, A.; Sergent, M. *Acta Crystallogr.* **1983**, *C39*, 1503.
(8) Perrin, C.; Chevrel, R.; Sergent, M.; Fisher, Ø. *Mater. Res. Bull.* **1979**, *14*, 1505.

10.1021/ic0512678 CCC: $33.50
Published on Web 12/21/2005

Table 1. Properties, VEC Values, and Developed Formulas of Selected Examples of Compounds Composed of M_6L_{14} Units (L = halogen or chalcogen)

compound	ref	unit	VEC	transport properties
		compounds based on discrete units or units interconnected by L^{a-a} ligands		
$Cs_2Mo_6Br_{14}$	13	$Mo_6Br^i_8Br^a_6$	24	insulating
$NaMo_6Br_{13}$	14	$Mo_6Br^i_8Br^{a-a}{}_{2/2}Br^a_4$	24	insulating
Mo_6Br_{12}	15	$Mo_6Br^i_8Br^{a-a}{}_{4/2}Br^a_2$	24	insulating
$Mo_6Br_{10}S$	16	$Mo_6S^iBr^i_7Br^{a-a}{}_{6/2}$	24	insulating
		compounds containing L^{i-a} and L^{a-i} interconnections developed in 1D, 2D, and 3D		
$Mo_6Br_6S_3$	6	$Mo_6Br^i_4S^{i-i}{}_{2/2}S^{i-a}{}_{2/2}Br^{a-a}{}_{4/2}S^{a-i}{}_{2/2}$ (1D)	24	semiconducting
$Re_6Se_8Cl_2$	7	$Re_6Se^i_4Se^{i-a}{}_{4/2}Cl^a_2Se^{a-i}{}_{4/2}$ (2D)	24	semiconducting
$Mo_6S_6Br_2$	8	$Mo_6Br^i_2S^{i-a}{}_{6/2}S^{a-i}{}_{6/2}$ (3D)	22	metallic, superconducting, $T_c = 13.8$ K
$PbMo_6S_8$	17	$Mo_6S^i_2S^{i-a}{}_{6/2}S^{a-i}{}_{6/2}$ (3D)	22	metallic, superconducting, $T_c = 14$ K
$Cs_{0.6}Mo_6S_7$	18	$Mo_6S^{i-i}{}_{2/2}S^{i-a}{}_{6/2}S^{a-i}{}_{6/2}$ (3D)	22	metallic, superconducting, $T_c = 8$ K.

electronic interactions between neighboring units (Table 1). These interactions are mainly the result of short M−L interunit distances, not direct M−M intercluster bonding. The ultimate term of condensation by L^{i-a}/L^{a-i} ligands is reached for the $Mo_6L^i_2L^{i-a}{}_{6/2}L^{a-i}{}_{6/2}$ (L = S, Se, Te) 3D framework that appears in the so-called Chevrel Phases, discovered in the early seventies by Sergent's group in Rennes.[9a] These latter series have only been obtained for Mo with the exception of the mixed metal clusters found in $Mo_2Re_4L_8$ and $Mo_4Ru_2L_8$.[9b] Many research works have been devoted to this class of compounds because of their remarkable physicochemical properties such as superconductivity at high-critical magnetic fields,[10] catalysis,[11] or redox intercalation.[12] In these compounds, the molecular character has disappeared to the benefit of a band structure with broadened valence bands and VEC values that can vary from 20 to 24. For 22 electrons per cluster, the Fermi level corresponds to a half-filled narrow band, and the superconducting properties of these compounds are optimum (i.e., $PbMo_6S_8$, $T_c = 14$ K).

A recent challenge was to obtain similar series based on M_6L_{18} units instead of M_6L_{14} units to learn more about the influence of the nature of the metal, ligand, and type of unit (M_6L_{18} or M_6L_{14}) on the electronic structures and physical properties. This goal has been reached in Nb_6 chemistry in which the replacement of inner halogens by oxygens favors stronger connections between $M_6L^i_{12}L^a_6$ units and enables a condensation by double O^{i-a}/O^{a-i} bridges similar to the L^{i-a}/L^{a-i} ones (L = S, Se, Te) observed for $M_6L^i_8L^a_6$ units. A large number of Nb_6 oxyhalides have been obtained[19] since the discovery of $ScNb_6Cl_{13}O_3$.[20] The presence of oxygen and halogen within the $Nb_6X_{18-x}O_x$ unit (X = Cl or Br) leads to important distortions of the cluster and to various electron counts (from 13 to 16) in relation to the significant discrepancy between the ionic radii and the charges of the oxygen and halogen atoms.[21] Furthermore, the condensation of Nb_6 oxychloride units through O^{i-a}, O^{a-i}, and O^{i-i} bridges stabilizes structures with topologies similar to those found in molybdenum chalcohalide chemistry. This is the case for $Na_{0.21}Nb_6Cl_{10.5}O_3$ that exhibits a O^{i-a}/O^{a-i} layered unit condensation,[19j] for $CsNb_6Cl_{12}O_2$ based on a O^{i-a}/O^{a-i} unit chain condensation,[19f] and more recently for $Nb_{10}Cl_{16}O_7$ based on Nb_6 octahedral clusters and Nb_2 pairs.[22] The ultimate term of condensation by O^{i-a}/O^{a-i} ligands has been obtained in $Ti_2Nb_6O_{12}$ which exhibits the same topology as Chevrel Phases with a O^{i-a}/O^{a-i} condensation in the three directions of space.[23]

We report here the synthesis and the crystal and electronic structures of the new $Na_2(Sc_4Nb_2)(Nb_6O_{12})_3$ niobium oxide whose structure is related to that of $Ti_2Nb_6O_{12}$. It is a new member of the larger $A_nBM_6L_{12}(Z)$ family (A = monovalent cation lying in tetrahedral cavities, B = monovalent or trivalent cations lying in octahedral cavities, M = rare earth, Zr, or Nb, Z = interstitial except for Nb). The structural relationships between the $A_nBM_6L_{12}(Z)$ series ($M_6L^i_{12}L^a_6$ unit-based compounds with a $M_6L^i_6L^{i-a}{}_{6/2}L^{a-i}{}_{6/2}$ cluster framework) and Chevrel Phases ($Mo_6L^i_8L^a_6$ unit-based compounds with a $Mo_6L^i_2L^{i-a}{}_{6/2}L^{a-i}{}_{6/2}$ cluster framework) are shown in terms of the M_6L_{18} and M_6L_{14} unit packing models. We particularly focus on the location of countercations within the cluster framework in relation to the type of units (M_6L_{14} or M_6L_{18}) and the compactness within the unit layer, as well as on the inner ligands involved in the inner−apical bridges.

(9) Chevrel, R.; Sergent, M. Superconductivity in Ternary Compounds. In *Topics in Current Physics*; Fischer, Ø, Maple, M. P., Eds.; Springer-Verlag: Berlin, 1982. (b) Perrin, A.; Sergent, M.; Fischer, Ø. *Mater. Res. Bull.* **1978**, *13*, 259.

(10) Fischer, Ø. *Appl. Phys.* **1978**, *16*, 1.

(11) Hilsenbeck, S. J.; McCarley, R. E.; Thompson, R. K.; Flanagan, L. C.; Schrader, G. L. *J. Mol. Catal. A* **1997**, *122*, 13.

(12) Tarascon, J.-M.; Di Salvo, F. J.; Murphy, D. W.; Hull, G. W.; Rietman, E. A.; Waszczak, J. V. *J. Solid State Chem.* **1984**, *54*, 204.

(13) Kirakci, K.; Cordier, S.; Perrin, C. *Z. Anorg. Allg. Chem.* **2005**, *631*, 411.

(14) Wang, P.; Xu, W.; Zheng, Y.-Q. *Solid State Sci.* **2003**, *5*, 573.

(15) Zheng, Y.-Q.; Grin, Yu. N.; von Schnering, H. G. *Z. Kristallogr.* **1998**, *213*, 469.

(16) Perrin, C.; Sergent, M.; Le Traon, F.; Le Traon, A. *J. Solid State Chem.* **1978**, *25*, 197.

(17) Guillevic, J.; Lestrat, H.; Grandjean, D. *Acta Crystallogr.* **1976**, *B32*, 1342.

(18) Gougeon, P.; Potel, M.; Padiou, J.; Sergent, M. *C. R. Acad. Sci.* **1983**, *297*, 339.

(19) Cordier, S.; Perrin, C.; Sergent, M. *Mater. Res. Bull.* **1996**, *31*, 683. (b) Cordier, S.; Perrin, C.; Sergent, M. *Mater. Res. Bull.* **1997**, *32*, 25. (c) Anokhina, E. V.; Essig, M. W.; Lachgar, A. *Angew. Chem., Int. Ed.* **1998**, *37*, 522. (d) Anokhina, E. V.; Day, C. S.; Essig, M. W.; Lachgar, A. *Angew. Chem., Int. Ed.* **2000**, *39*, 1047. (e) Anokhina, E. V.; Day, C. S.; Lachgar, A. *Chem. Commun.* **2000**, 1491. (f) Gulo, F.; Perrin, C. *J. Mater. Chem.* **2000**, *10*, 1721, (g) Gulo, F.; Roisnel, T.; Perrin, C. *J. Mater. Chem.* **2001**, *11*, 1237. (h) Anokhina, E. V.; Day, C. S.; Lachgar, A. *Inorg. Chem.* **2001**, *40*, 507. (i) Anokhina, E. V.; Duraisamy, T.; Lachgar, A. *Chem. Mater.* **2002**, *14*, 4111. (j) Gulo, F.; Perrin, C. *J. Solid State Chem.* **2002**, *163*, 325.

(20) Cordier, S.; Perrin, C.; Sergent, M. *Eur. J. Solid State Inorg. Chem.* **1994**, *31*, 1049.

(21) Cordier, S.; Gulo, F.; Perrin, C. *Solid State Sci.* **1999**, *1*, 637.

(22) Cordier, S.; Gulo, F.; Roisnel, T.; Gautier, R.; Le Guennic, B.; Halet, J.-F.; Perrin, C. *Inorg. Chem.* **2003**, *42*, 8320.

(23) Anokhina, E. V.; Essig, M. W.; Day, C. S.; Lachgar, A. *J. Am. Chem. Soc.* **1999**, *121*, 6827.

We also show that despite a topology similar to that encountered in Chevrel Phases, intercalation properties are not expected in the $Nb_6O^i{}_6O^{i-a}{}_{6/2}O^{a-i}{}_{6/2}$ cluster framework-based compounds. Finally, it is shown, from theoretical LMTO calculations, that a maximum VEC of 14 can be reached in a $Nb_6O^i{}_6O^{i-a}{}_{6/2}O^{a-i}{}_{6/2}$ cluster framework, leading to semiconducting behavior.

Experimental Section

Synthesis and Chemical Analyses. $Na_2(Sc_4Nb_2)(Nb_6O_{12})_3$ was prepared from Nb_2O_5, NbO, Sc_2O_3, and NaF starting materials with a 1:4:1:3 ratio. Powders were weighed, ground, formed into a pellet under inert atmosphere, and placed into an open niobium container (Plansee). The tube was encapsulated in an evacuated silica ampule which was subsequently placed in a furnace and brought up to 950 °C in 24 h. After 96 h, the tube was cooled to room temperature within 12 h. At this stage the quartz ampule was white and very brittle because of the attack and crystallization of silica. The remaining bulk product, inside the niobium tube, was then washed with distilled water and HF in an ultrasonic bath to eliminate the excess NaF and soluble impurities. The X-ray powder diffraction patterns of the resulting powder revealed supplementary lines attributed to the presence of NbO as an impurity. Many experiments were performed to improve the yield of the reaction. Unfortunately, it turned out that the modification of the loaded stoichiometries did not lead to purer samples since the increase of the Nb_2O_5 starting composition favored the formation of $ScNbO_4$ ternary oxide.[24] On the other hand, the use of an alumina container instead of a niobium crucible strongly decreased the yield of the reaction. Further attempts to synthesize other $Na_y(Sc_{2-x}Nb_x)Nb_6O_{12}$ oxides starting from $NaNbO_4$ mineralizers[25] failed. The attack of the glass container clearly indicated a reaction between the niobium container and SiO_2 to form Nb_5Si_3[26] and NbO. However, no trace of Nb_5Si_3 was found in the X-ray powder pattern of the bulk compound or the presence of the remaining fluoride. The presence of NbO in the final compound could not be avoided even by modification of the starting loaded stoichiometries.

Accurate WDS−EPMA (wavelength dispersive X-ray spectrometers−electron probe microanalyzer) measurements have been performed using a Camebax SX 50 microprobe, equipped with five spectrometers and a variety of crystals to make the radiation characteristics of the full range of elements (atomic weight greater than that of He) accessible. Several single-crystals of the title compound from several preparations were embedded in epoxy resin and polished down to 0.25 mm diamond grade to obtain a perfect plane surface. The measurements were performed on several points of each crystal (total 75 points). Each of them exhibits Na, Sc, Nb, and O, but no trace of fluorine was detected. The experimental average composition determined from these measurements is $Na_{2.3(1)}Sc_{3.5(1)}Nb_{19.4(3)}O_{36.7(3)}$. This formula is close to $Na_2Sc_4Nb_{20}O_{36}$ ($Na_2(Sc_4Nb_2)(Nb_6O_{12})_3$) and was confirmed by structural determination and electronic considerations. As already observed for several other niobium cluster oxides, the presence of fluoride salt as a mineralizer does not lead to the incorporation of fluorine into the crystal lattice. Some exceptions have to be mentioned for example $KNb_8O_{14-x}F_x$ ($x \approx 1.0$)[27] and $K_4Al_2Nb_{11}O_{21}F$.[28]

Table 2. Crystal Data and Conditions of Data Collection for $Na_2Sc_4Nb_{20}O_{36}$ ($Na_2(Sc_4Nb_2)(Nb_6O_{12})_3$)

formula	$Na_2Sc_4Nb_{20}O_{36}$
temp (K)	298
fw (g/mol)	2660.02
cryst size (mm^3)	0.025 × 0.024 × 0.02
crystal syst	trigonal
space group	$R\bar{3}$ (No. 148)
a (Å)	8.0335(3)
c (Å)	14.5718(5)
V ($Å^3$)	814.43(5)
Z	1
d_{calcd} (g/cm^3)	5.424
μ (mm^{-1})	7.642
no. of reflns integrated	5688
R_{int}	0.0442
no. of independent reflns	925
no. of independent reflns $I > 2\sigma(I)$	728
Θ_{min}, θ_{max}	3.24°, 36.96°
h	−13 → 13
k	−12 → 13
l	-24 → 24
data/restraints/paramrs	925/0/44
R_1 ($I > 2\sigma(I)$)[a]	0.028
R_2 (all data)[a]	0.050
GOF	1.09
$\Delta\rho$ max, min ($e/Å^3$)	1.90, −1.61

[a] $R_1 = \sum_{hkl}|F_o - F_c|/\sum_{hkl}|F_o|$; $R_2 = [\sum_{hkl}[w(F_o^2 - F_c^2)^2]/\sum_{hkl}[w(F_o^2)^2]]^{1/2}$.

Structure Determination by Single-Crystal X-ray Diffraction. A suitable single-crystal of the title compound was mounted on a Nonius KappaCCD X-ray area-detector diffractometer with Mo Kα radiation ($\lambda = 0.71073$ Å). Details of the data collection are reported in Table 2. Once the data processing was performed by the KappaCCD analysis software,[29] the cell parameters were refined as follows: $a = 8.0335(3)$ Å, $c = 14.5718(5)$ Å, $V = 814.43(5)$ $Å^3$. Let us note that the analysis of several other single crystals from different batches led to the same refined lattice parameters within the standard errors. The calculation of E statistics[30] performed on the data suggested a centrosymmetric space group. According to the observed systematic extinctions, the structure was solved in the $R\bar{3}$ space group by direct methods using SIR97.[31] Structural refinements against F^2 by least-squares techniques, combined with Fourier difference syntheses, were performed using SHELXL-97.[32] Nb from the Nb_6 cluster and oxygen atoms fully occupy three 18*f* positions and have been refined anisotropically. In a first step, it was assumed that scandium fully occupied a 6*h* position, but after several cycles of refinements, it turned out that an electronic peak remained close to this position. Nb2 was then introduced on this residue with the same atomic displacement parameter as Sc2. The sum of the occupancies of Sc2 and Nb2 was restricted to the value corresponding to a fully occupied 6*h* position. Afterward, the first two restraints were progressively relaxed during the convergence, leading to final positions in agreement with reliable Sc−O and Nb−O interatomic distances. Because of the lower occupancy of Nb2 compared to Sc2, this atom was refined isotropically. The structure was then solved for several crystals from different

(24) Inorganic Crystal Structure Database, Fachinformationzentrum (FIZ) Karlsruhe, CSD 24-1013.
(25) Geselbracht, M. J.; Stacy, A. M. *J. Solid State Chem.* **1994**, *110*, 1.
(26) Parthe, E.; Lux, B.; Novotny, H. *Monatsh. Chem.* **1955**, *86*, 859.
(27) Köhler, J.; Tischtau, R.; Simon, A. *J. Chem. Soc., Dalton Trans.* **1991**, 829.
(28) (a) Simon, A.; Köhler, J.; Tischtau, R.; Miller, G. *Angew. Chem.* **1989**, *101*, 1695. (b) Köhler, J.; Svenson, G.; Simon, A. *Angew. Chem., Int. Ed. Engl.* **1992**, *31*, 1437.
(29) COLLECT, DENZO, SCALEPACK, and SORTAV. *Kappa CCD Program Package*; Nonius B. V.: Delft, The Netherlands, 1999.
(30) Marsh. R. E. *Acta Crystallogr.* **1999**, *B51*, 897.
(31) Cascarano, G.; Altomare, A.; Giacovazzo, C.; Guagliardi, A.; Moliterni, A. G. G.; Siliqi, D.; Burla, M. C.; Polidori, G.; Camalli, M. *Acta Crystallogr.* **1996**, *A52*, C-79.
(32) Sheldrick, G. M. *SHELXL-97: Program for the Refinement of Crystal Structure*; University of Göttingen: Göttingen, Germany, 1997.

Table 3. Atomic Coordinates and Atomic Displacement Parameters

atom	Wyckoff	occupancy	*x*	*y*	*z*	U_{eq} (Å^2)[a]
Nb1	18*f*	1	0.21522(3)	0.18934(3)	0.077003(17)	0.00444(8)
O1	18*f*	1	0.0284(3)	0.2124(3)	0.17160(13)	0.0072(3)
O2	18*f*	1	0.2453(3)	0.1616(3)	0.33814(12)	0.0085(4)
Nb2	6*c*	0.327(5)	0	0	0.2675(7)	0.0053(14)
Sc2	6*c*	0.673(5)	0	0	0.2746(8)	0.0043(9)
Na	18*f*	0.11	0.261(6)	0.614(14)	0.1560(19)	0.024(5)

[a] $U_{eq} = {}^1/_3\sum_i\sum_j (U^{ij}a^i a^j \vec{a}_i\cdot\vec{a}_j)$ except for Nb2, refined isotropically, in which case the isotropic displacement parameter is given.

Table 4. Selected Interatomic Distances (Å) in $Na_2Sc_4Nb_{20}O_{36}$[a]

Nb1−Nb1 × 6	2.7766(4)	Sc2−O2 × 3	1.967(6)
Nb1−Nb1 × 6	2.8318(4)	Sc2−O1 × 3	2.197(8)
Nb1−O2	2.035 (2)	Nb2−O2 × 3	2.017(6)
Nb1−O2	2.102(2)	Nb2−O1 × 3	2.128(7)
Nb1−O1^i	2.113(2)	Nb1−Nb2	3.2128(6)
Nb1−O1^i	2.141(2)	Nb1−Nb2	3.222(9)
Nb1−O1^a	2.254(2)	Nb1−Sc2	3.2197(10)
Nb1−$Nb1_{intercluster}$	3.213	Nb1−Sc2	3.2198(9)

[a] O1^i and O1^a refer to the inner and apical ligands, respectively.

preparations, and the Sc/Nb ratio on the tetrahedral site of units (see discussion below) did not deviate within the standard errors to 2/3:1/3. The niobium, scandium, and oxygen contents correspond to $Sc_4Nb_{20}O_{36}$. The Na cation was found to be statistically distributed on six equivalent crystallographic positions, almost merged with the *ab* plane, around the origin of the unit cell, and corresponding to each other by a −3 symmetry operation. Because of the partial occupation and small weight of Na cation, the combined refinement of its occupation and atomic displacement parameters led to unrealistic physical values. According to the chemical analyses, the occupation was subsequently restricted to 2 Na atoms per formula. This strategy led to reasonable atomic displacement parameters. Moreover, the value of two sodium atoms per formula corresponds to an electron count that has been corroborated by LMTO calculations. Positional parameters and interatomic distances are given in Tables 3 and 4, respectively.

DFT Computations. Self-consistent ab initio band structure calculations were performed on $Ti_2Nb_6O_{12}$ and $Na_2(Sc_4Nb_2)(Nb_6O_{12})_3$ with the scalar relativistic tight-binding linear muffin-tin orbital (LMTO) method in the atomic spheres approximation including the combined correction.[33] Because of the fractional occupation of the Nb2 and Sc2 crystallographic positions, several $Na_2(Sc_4Nb_2)(Nb_6O_{12})_3$ model compounds were considered. Exchange and correlation were treated in the local density approximation using the von Barth−Hedin local exchange correlation potential.[34] Within the LMTO formalism interatomic spaces were filled with interstitial spheres. The optimal positions and radii of these additional "empty spheres" (ES) were determined by the procedure described in ref 35. Six and forty-nine nonsymmetry-related ES with $0.76 \le r_{ES} \le 2.40$ Å and $0.81 \le r_{ES} \le 2.39$ Å were introduced for the calculations of $Ti_2Nb_6O_{12}$ and $Na_2(Sc_4Nb_2)(Nb_6O_{12})_3$, respectively. The full LMTO basis set consisted of 5s, 5p, 4d, and 4f functions for Nb spheres, 4s, 3p, and 3d for Sc and Ti spheres, 3s, 2p, and 3d functions for O spheres, and s, p, and d functions for ES. The eigenvalue problem was solved using the following minimal basis set obtained from the Löwdin downfolding technique: Nb 5s, 5p, and 4d; Sc 4s and 3d; Ti 4s, 4p, and 3d; Na 3s; O 2p; and interstitial 1s LMTOs. The *k*-space integration was performed using the tetrahedron method.[36] Charge self-consistency and average properties were obtained from 90 and 72 irreducible *k* points for the calculations of $Ti_2Nb_6O_{12}$ and $Na_2(Sc_4Nb_2)(Nb_6O_{12})_3$, respectively. A measure of the magnitude of the bonding was obtained by computing the crystal orbital Hamiltonian populations (COHP) which are the Hamiltonian population weighted density of states (DOS).[37] As recommended, a reduced basis set (in which all ES LMTO's were downfolded) was used for the COHP calculations.[38] Bands, DOS, and COHP curves were shifted so that ϵ_F lies at 0 eV.

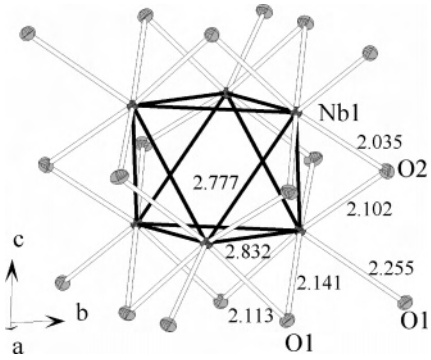

Figure 1. Representation of the $Nb_6O^i{}_6O^{i-a}{}_{6/2}O^{a-i}{}_{6/2}$ unit. Displacement ellipsoids are shown at the 50% probability level. Bond lengths are in angstroms.

Results and Discussion

Description of the Structure. The $Na_2(Sc_4Nb_2)(Nb_6O_{12})_3$ oxide crystallizes in the trigonal system, rhombohedral lattice, space group $R\bar{3}$. Within the associated hexagonal unit cell, the stoichiometry is $Na_2Sc_4Nb_{20}O_{36}$ written as $Na_2(Sc_4Nb_2)(Nb_6O_{12})_3$ to show the cluster unit. On the other hand, within the rhombohedral unit cell, the latter stoichiometry becomes $Na_{0.66}(Sc_{1.33}Nb_{0.66})Nb_6O_{12}$ and will be used in the following for the sake of comparison to that of $Ti_2Nb_6O_{12}$. The structure is built up from Nb_6O_{18} anionic units of symmetry −3 centered on a 3*b* Wyckoff position (Figure 1). The Nb_6O_{18} units are stacked according to a cubic-close-packed mode following an ABC sequence that generates the tetrahedral and octahedral cavities of units occupied by the cations. In $Ti_2Nb_6O_{12}$, the tetrahedral cavities are occupied by titanium cations (Ti^{IV}), whereas the octahedral cavities are empty. In $Na_{0.66}(Sc_{1.33}Nb_{0.66})Nb_6O_{12}$, the tetrahedral cavities are randomly occupied by scandium and niobium (Nb^V), and the octahedral ones are statistically occupied by sodium. The units shared common oxygen ligands to form a tridimensional framework with the $Nb_6O^i{}_6O^{i-a}{}_{6/2}O^{a-i}{}_{6/2}$ developed formula. Note that this framework is topologically related to that of $Mo_6L^i{}_2L^{i-a}{}_{6/2}L^{a-i}{}_{6/2}$, based on Mo_6L_{14} units, obtained in Chevrel Phases. Compared to $Ti_2Nb_6O_{12}$, the analysis of the intraunit distances reported in Table 4 for

(33) (a) Andersen, O. K. *Phys. Rev. B* **1975**, *12*, 3060. (b) Andersen, O. K. *Europhys. News* **1981**, *12*, 4. (c) Andersen, O. K. In *The Electronic Structure Complex Systems*; Phariseau, P., Temmerman, W. M., Eds.; Plenum Publishing Corporation: New York, 1984. (d) Andersen, O. K.; Jepsen, O. *Phys. Rev. Lett.* **1984**, *53*, 2571. (e) Andersen, O. K.; Jepsen, O.; Sob, M. In *Electronic Band Structure and its Application*; Yussouf, M., Ed.; Springer-Verlag: Berlin, 1986. (f) Skriver, H. L. *The LMTO Method*; Springer-Verlag: Berlin, 1984.
(34) von Barth, U.; Hedin, L. *J. Phys. C* **1972**, *5*, 1629.
(35) Jepsen, O.; Andersen, O. K. *Z. Phys. B* **1995**, *97*, 35.
(36) Blöchl, P. E.; Jepsen, O.; Andersen, O. K. *Phys. Rev. B* **1994**, *49*, 16223.
(37) Dronskowski, R.; Blöchl, P. E. *J. Phys. Chem.* **1993**, *97*, 8617.
(38) Boucher, F.; Rousseau, R. *Inorg. Chem.* **1998**, *37*, 2351.

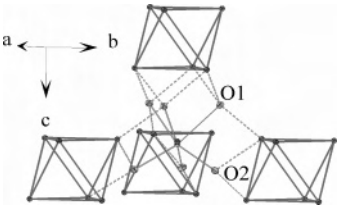

Figure 2. Local environment of the Sc^{3+} and Nb^{5+} cations in the tetrahedral cavity. For clarity, only the ligands involved in the coordination sphere of the cations are represented. Displacement ellipsoids are shown at the 50% probability level.

$Na_{0.66}(Sc_{1.33}Nb_{0.66})Nb_6O_{12}$ reveals an elongation of the Nb−O^a bond lengths and a contraction of the Nb−Nb bond lengths, whereas the Nb−O^i distances are fairly similar ($Ti_2Nb_6O_{12}$: Nb−Nb = 2.8502 (4) Å, Nb−Nb = 2.7896(4) Å, Nb−$O1^i$ = 2.076(2) Å, Nb−$O1^i$ = 2.142(2) Å, Nb−$O1^a$ = 2.212(2) Å, Nb−O2 = 2.051(2) Å, Nb−O2 = 2.113(2) Å). Thus, the slight variation of bond lengths going from $Ti_2Nb_6O_{12}$ to $Na_{0.66}(Sc_{1.33}Nb_{0.66})Nb_6O_{12}$ must be attributed to a different repartition of the cationic charges within the $Nb_6O^i{}_6O^{i-a}{}_{6/2}O^{a-i}{}_{6/2}$ anionic framework, as already found for M_6X_{18}-based compounds, as well as a distortion of the unit cell. Let us recall that a complete study of the evolution of bond lengths in M_6X_{18} anionic units versus the charge repartition was performed for the $A_xREM_6X_{18}$ series (A = alkaline earth; RE = rare earth; M = Nb, Ta; X = Cl, Br).[39]

Substitution of Sc and Nb atoms for Ti atoms as well as occupation of the octahedral cavities by Na, which are not occupied in $Ti_2Nb_6O_{12}$, leads to an increase of the cell parameters (a = 7.9364(5) Å, c = 14.4339(10) Å and a = 8.0335(3) Å, c = 14.5718(5)) Å for $Ti_2Nb_6O_{12}$ and $Na_{0.66}(Sc_{1.33}Nb_{0.66})Nb_6O_{12}$, respectively). Nb2 and Sc2 are randomly distributed according to a 1/3:2/3 ratio on the ternary axis in the tetrahedral cavities of units on two close 6*c* Wyckoff positions shifted above the centroid of the tetrahedron (0 0 $^1/_4$). The atomic coordination level of these cations is not tetrahedral but octahedral. Indeed, the distorted octahedral coordination of Sc2 and Nb2 (Figure 2) is built up from three inner oxygen ligands belonging to three adjacent clusters and from three other inner−apical ligands belonging to one adjacent cluster (Nb2−O1 = 2.129 Å × 3 and Nb2−O2 = 2.017 Å × 3; Sc2−O1 = 2.198 Å × 3 and Sc2−O2 = 1.967 Å × 3). The site of Nb2 is then less distorted than that of Sc2. Na^+ cations statistically occupy the octahedral cavities of units (Figure 3a and b) generated by the stacking of the cluster units. A large twelve coordination site of ligands is generated around the origin of the unit cell by the oxygen ligands belonging to the six units building the octahedral cavity (Figure 3). The sodium cation is shifted from the origin that merges with the centroid of the octahedral cavity and statistically (11.11%) occupies a 18*f* Wyckoff position. Because of the statistical occupancy of the sodium positions, the bond lengths obtained by X-ray structural investigation correspond to an average between empty and full sites. As indicated in Table 6, if Na was located on the centroid of the octahedral cavity, it will be surrounded by six O^i and six O^{i-a} units (O−O^i = 2.928 Å and O−O^{i-a} = 3.218 Å, respectively). The shift from the centroid allows shorter Na−O contacts and a lower coordination number. Such complex coordination is usual for alkali ions and has been already observed in the $A_xREM_6L_{18}$ series (A = alkali ion, RE = rare earth, M = Nb or Ta, L = halogen or (halogen and oxygen)).[4,5]

Theoretical Considerations. A previous theoretical study on the electronic structure of $Ti_2Nb_6O_{12}$ using extended Hückel theory (EHT) calculations has been reported.[23] In this compound, the metallic electron count of the octahedral Nb_6 cluster is equal to 14. The total density of states (DOS) computed depicts narrow peaks that are typical of weak interactions between the Nb_6 clusters. Indeed insignificant Ti−Nb and intercluster Nb−Nb bondings have been computed. Because of the nonbonding character of the empty band that lies around half an electronvolt above the Fermi level, the authors suggested that the reduction of this compound could be achieved.

To analyze the role of the isolated Sc2, Nb2, and Na atoms in the title compound, periodic density functional theory (DFT) calculations were carried out. For the sake of comparison, similar calculations were performed on Ti_2-

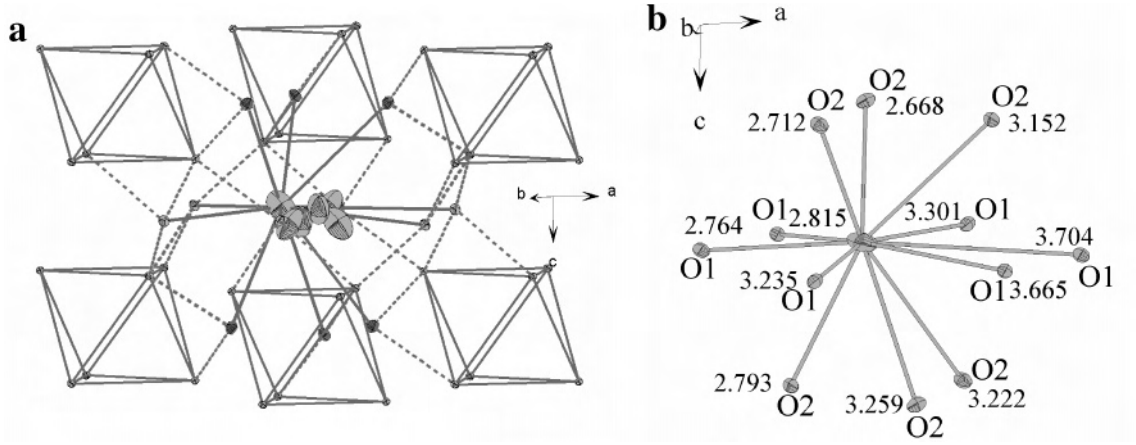

Figure 3. (a) Local environment of the Na^+ cation in the octahedral cavity. The crystallographic positions represented are statistically occupied by Na^+ (11.11% in the whole structure). For clarity, only the ligands involved in the coordination sphere of the cation are represented. Displacement ellipsoids are shown at the 50% probability level. (b) Local coordination sphere of Na^+. Note that, because of the statistical occupancy of the sodium positions, the indicated bond lengths (Å) correspond to an average between the empty and full sites.

Table 5. Unit-Cell Parameters and Selected Distances (Å) in Binary and Ternary Chevrel Phases[a]

compound ref	VEC	rhombohedral unit-cell params	hexagonal unit-cell params	L^i-L^i	O−ccluster	O−fccluster	$O-L^i$	$O-L^{i-a}$	$T-L^i$
Mo_6S_8 44	20	$a = 6.432$ $\alpha = 91.57$	$a = 9.220$ $c = 10.831$ $c/a = 1.17$	4.703 ($2rS^{2-} = 3.68$	5.621	5.416	2.352	3.154	0.356
Mo_6Se_8 45	20	$a = 6.658$ $\alpha = 91.58$	$a = 9.544$ $c = 11.208$ $c/a = 1.17$	4.792 ($2rSe^{2-} = 3.96$)	5.819	5.605	2.396	3.191	0.407
Mo_6Te_8 46	20	$a = 7.048$ $\alpha = 92.472$	$a = 10.179(1)$ $c = 11.674(2)$ $c/a = 1.14$	4.877 ($2rTe^{2-} = 4.42$)	6.191	5.837	2.438	3.369	0.480
$PbMo_6S_8$ 17	22	$a = 6.544$ $\alpha = 89.48$	$a = 9.212$ $c = 11.436$ $c/a = 1.24$	5.752		5.718	2.786	3.121	
$PbMo_6Se_8$ 17	22	$a = 6.810$ $\alpha = 89.23$	$a = 9.565$ $c = 11.951$ $c/a = 1.24$	5.790		5.975	2.895	3.205	
$Cu_{1.38}Mo_6S_8$ 47	22	$a = 6.559$ $\alpha = 95.512$	$a = 9.713$ $c = 10.213$ $c/a = 1.05$	4.126	5.860	5.107	2.063 Cu1 2.430, 2.453 Cu2 2.246	3.442 Cu1 2.354, 2.349 Cu2 2.295, 2.383, 2.577	0.490

[a] The O and T labels define the centroids of the octahedral and tetrahedral cavities.

Table 6. Unit-Cell Parameters and Selected Distances in $A_nM_6L_{12}(Z)$ Compounds

compound ref	rhombohedral unit-cell params	hexagonal unit-cell params	O−ccluster	O−fccluter	$O-X^i$	$T-X^i$	T−M
$NaLa_6I_{12}Os$ 43	$a = 10.07$ $\alpha = 107.1°$	$a = 16.214$ $c = 11.172$ $c/a = 0.72$	9.545 × 6	5.586 × 2	3.214 × 6	2.785 × 3	2.591 × 3
$CsEr_6I_{12}C$ 42	$a = 9.41$ $\alpha = 72.47°$	$a = 11.120$ $c = 20.38$ $c/a = 1.85$	7.285 × 6	10.31 × 2	4.20^{i-a} × 6 4.161^{a-i} × 6	2.958^{ia} × 3 2.985^{i} × 3	4.514 × 3 4.267 × 3
$Ti_2Nb_6O_{12}$ 23	$a = 6.64$ $\alpha = 73.31°$	$a = 7.9364$ $c = 14.4339$ $c/ac/a = 1.82$	5.175	7.217	2.919^{i} × 6 3.217^{i-a} × 6	1.901 × 3 2.059 × 3	2.798 × 3 3.165 × 3
$Na_{0.66}(Sc_{1.33}Nb_{0.66})Nb_6O_{12}$ this work	$a = 6.78$ $\alpha = 72.61°$	$a = 8.03$ $c = 14.845$ $c/a = 1.85$	5.233 × 6	7.273 × 2	2.928^{i} × 6 3.218^{i-a} × 6	1.973 × 3 2.156 × 3	3.000 × 3 3.210 × 3

Nb_6O_{12}. Total and various atom-projected DOS curves for $Ti_2Nb_6O_{12}$ are sketched in Figure 4. Both the DFT and EHT DOS computed for $Ti_2Nb_6O_{12}$ are very comparable.[23] In the vicinity of the Fermi level, the main difference lies in the relative position of the vacant peak that derives from the "a_{2u}" molecular orbital (MO) of the octahedral Nb_6 cluster as well as the d orbitals of Ti. They overlap in energy according to DFT calculations, whereas they are somewhat separated by a small energy gap of ca. 0.2 eV with the EHT calculations. The COHP curves, sketched in Figure 4, show that the lower part of these lowest-unoccupied bands present a Nb−Nb bonding character, as already noticed with the EHT method. On the other hand, an Nb−Ti antibonding character is also computed for these bands as well as a weak antibonding Nb−O character and a strong Ti−O antibonding character. Therefore, assuming a rigid band model, occupation of these bands is unfavorable. This partly explains why attempts to reduce this compound have been unsuccessful so far.[23]

Because of the fractional occupation of the Na, Nb2, and Sc2 crystallographic positions, a lower symmetry had to be considered for the calculations of the band structure of $Na_2(Sc_4Nb_2)(Nb_6O_{12})_3$. All of the different atomic distributions of the Sc2 and Nb2 atoms were computed. Because of the similarity of the results, only one is discussed. Total and various atom-projected DOS and COHP computed for several atomic contacts in the structure are sketched in Figures 5 and 6, respectively. The bands that lie between −1.5 eV and the Fermi level are mainly centered on the Nb_6 octahedra with metal−metal bonding character. A small energy gap of ca. 0.25 eV separates these occupied bands from the lowest-vacant bands that show a major Nb2 contribution and a minor Nb_6 character. These latter bands are overall metal−metal nonbonding in the Nb_6 octahedron but significantly Nb2−Nb (octahedron) antibonding. Moreover, these bands show an antibonding metal−oxygen character (not shown here). Therefore, their occupation is unfavorable leading to an idealized electron count of 14 per cluster. This is consistent with the fractional occupation of the Na site as well as the refined value of 1/3 for the Sc2/Nb2 ratio to reach this optimized electron count. Because of the occurrence of a small band gap, semiconducting behavior is expected for this compound.

Unit Stacking in $A_nM_6L_{12}(Z)$ Series and in Chevrel Phases ($A_xMo_6L_8$). $Na_{0.66}(Sc_{1.33}Nb_{0.66})Nb_6O_{12}$ is a new member of the large $A_nBM_6L_{12}(Z)$ family (A = monovalent cation lying in tetrahedral unit cavities, B = monovalent or trivalent cations lying in octahedral unit cavities, M = rare earth, Zr, or Nb, Z = interstitial when M = rare earth or Zr). We propose here to show the structural correlation between the $Na_{0.66}(Sc_{1.33}Nb_{0.66})Nb_6O_{12}$ oxide and more generally between the $A_nBM_6L_{12}(Z)$ series ($M_6L^i{}_{12}L^a{}_6$ units building a $M_6L^i{}_6L^{i-a}{}_{6/2}L^{a-i}{}_{6/2}$ cluster network) and the Chevrel Phases ($Mo_6L^i{}_8L^a{}_6$ units building a $Mo_6L^i{}_2L^{i-a}{}_{6/2}L^{a-i}{}_{6/2}$ cluster

(39) Perrin, C.; Cordier, S.; Ihmaïne, S.; Sergent, M. *J. Alloys Compd.* **1995**, *229*, 123.

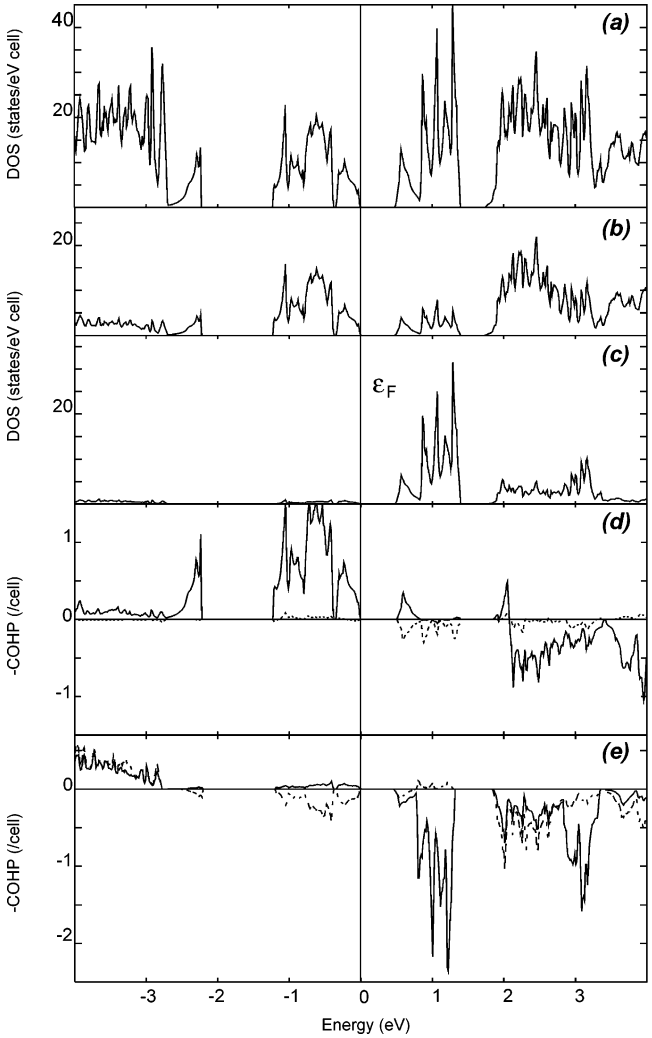

Figure 4. LMTO calculations for $Ti_2Nb_6O_{12}$: (a) Total DOS, (b) Nb-projected DOS, (c) Ti-projected DOS, (d) COHP curves for Nb−Nb contacts within the Nb_6 cluster (plain) and for Nb−Ti contacts (dotted) ranging from 3.18 to 3.27 Å, and (e) COHP curves for Ti−O contacts (plain) ranging from 1.87 to 2.12 Å and for Nb−O contacts (dotted) ranging from 2.05 to 2.21 Å.

network) in terms of M_6L_{18} and M_6L_{14} unit packing models. Let us note that the packing in the structures of $Zr_6L_{12}(Z)$[40,41] and related $A_nM_6L_{12}(Z)$ series[42,43] have already been described in term of a L anion packing.[23] However, since the L ligands are bonded to the clusters to form larger rigid anionic units, this model is not fully satisfactory for discussion.

Both Chevrel Phases and $A_nBM_6L_{12}(Z)$ series are based on octahedral M_6 clusters centered on the apexes of a rhombohedral unit cell (Figure 7). Each cluster is linked to six adjacent clusters, three above and three below, via six inner−apical and six apical−inner bridges along the edges of the rhombohedral unit cell. This latter results from a cubic close packing of unit layers (ABCA sequences) along the 3-fold axis that generates two tetrahedral cavities and one

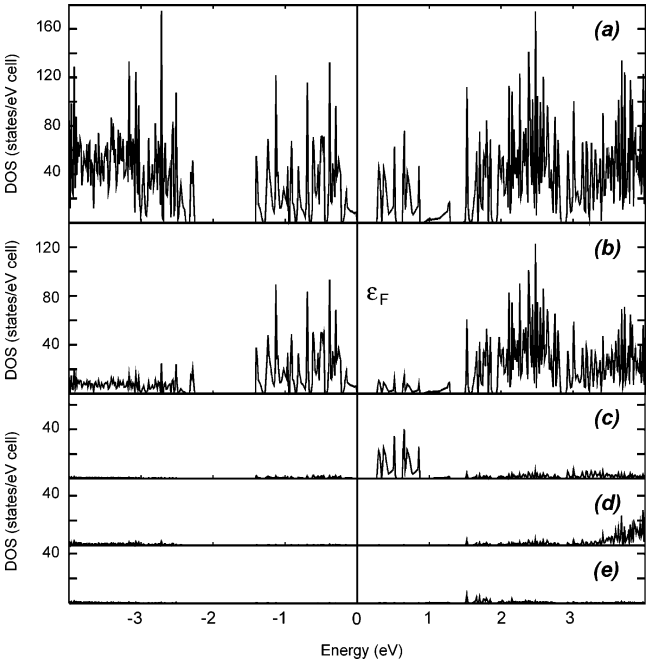

Figure 5. LMTO calculations for $Na_2(Sc_4Nb_2)(Nb_6O_{12})_3$: (a) Total DOS, (b) Nb of Nb_6 cluster contribution, (c) Nb2 contribution, (d) Sc contribution, and (e) Na contribution.

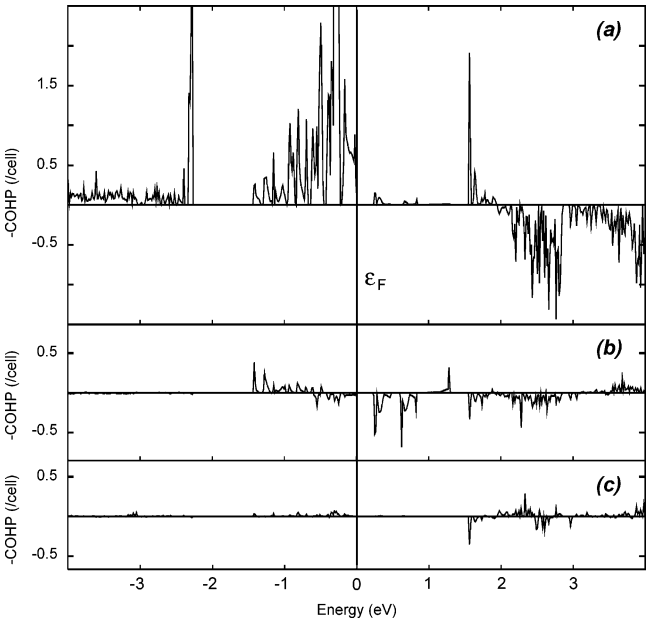

Figure 6. LMTO calculations for $Na_2(Sc_4Nb_2)(Nb_6O_{12})_3$: COHP curves for (a) Nb−Nb contacts within Nb_6 cluster, (b) Nb2−Nb of the Nb_6 cluster ranging from 3.21 to 3.22 Å, and (c) Sc−Nb of the Nb_6 cluster ranging from 3.21 to 3.31 Å.

octahedral cavity of cluster units in the rhombohedral unit cell (Figure 7). In the following, the clusters building the octahedral cavity will be labeled c-cluster and the two additional ones which face-cap the octahedron to build the rhombohedral unit cell will be labeled fc-cluster. A useful tool for comparison of the compactness in the rhombohedral unit cell is the distance between the O or T positions with the center of adjacent c-clusters and fc-clusters (O and T define the centroids of the cavities generated by the units). Countercations are located in the tetrahedral and octahedral cavities and their positions can either merge with those of

(40) Corbett, J. D.; Daake, R. L.; Poeppelmeier, K. R.; Guthrie, D. H. *J. Am. Chem. Soc.* **1978**, *100*, 652.
(41) Smith, J. D.; Corbett, J. D. *J. Am. Chem. Soc.* **1985**, *107*, 5704.
(42) Artelt, H. M.; Schleidt, T.; Meyer, G. *Z. Anorg. Allg. Chem.* **1992**, *618*, 18.
(43) Uma, S.; Corbett, J. D. *J. Solid State Chem.* **2001**, *161*, 161.

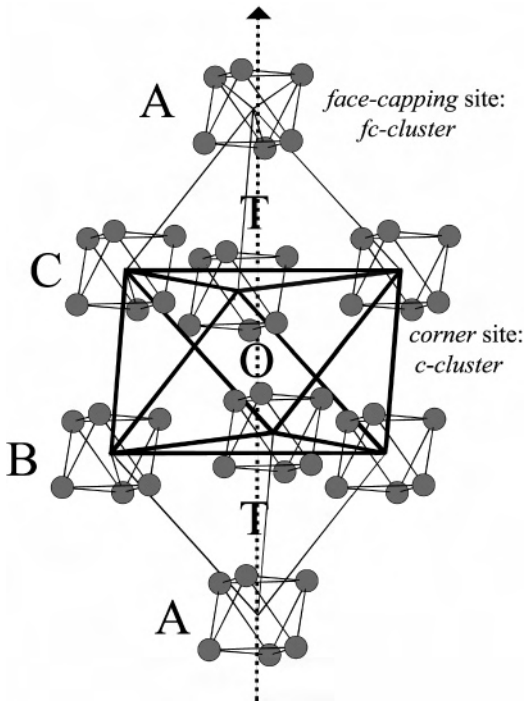

Figure 7. Representation of the common skeleton in Chevrel Phases and in the $A_nM_6L_{12}(Z)$ series. This cell is built up from six c-clusters at the corner of the octahedron and two additional fc-clusters. Two tetrahedral cavities and one octahedral cavity are generated in this rhombohedral cell. The T and O labels refer to the centroids of these cavities.

the T and O centroids or be slightly shifted. The occupation of these cavities by countercations depends on the distortion of the rhombohedral unit cell in relation with the type of units (M_6L_{14} or M_6L_{18}), the compactness within the unit layer, and the type of ligands involved in the coordination sphere of cations.

Unit Condensation and Octahedral and Tetrahedral Cavities in Chevrel Phases. In the following, we will focus on the matrix and steric effects of ligands on the stacking and cavity sizes. The VEC variations that influence the Mo−Mo intracluster distances can be neglected compared to the aforementioned effects. The condensation mechanism between two adjacent units in Chevrel Phases (rhombohedral unit cell) is represented in Figure 8a. The unit of −3 symmetry is oriented in such a way that the two inner X^i ligands located on the ternary axis are not involved in the interunit bridges. Selected interatomic distances in Chevrel Phases and in the $A_nM_6L_{12}(Z)$ series are reported in Tables 5 and 6, respectively.

Binary Compounds: Mo_6S_8, Mo_6Se_8, and Mo_6Te_8. In binary compounds of general formula Mo_6L_8 ($Mo_6L^i{}_2L^{i-a}{}_{6/2}L^{a-i}{}_{6/2}$), the position of the T centroid quasi-merges with that of the L^i inner ligands, and consequently, no vacant cationic site can be considered in the tetrahedral cavity even by a shift of cations. The layers, stacked along the ternary axis, are strongly interpenetrated as shown by the values of the *c*/*a* ratio (see Table 5) which are lower than those theoretically observed in close compact structures (1.73). The O−c-cluster distances are longer than the O−fc-cluster ones. The first coordination sphere around the O centroid is formed by two L^i ligands belonging to the two fc-clusters and six X^{i-a} ligands belonging to the six c-clusters. As expected, the L^i-L^i interatomic distance decreases going from Te to S, but this decrease is smaller than expected when considering only the ionic radii of the chalcogens. In other words, the smaller the chalcogen, the larger the size of the vacant site. Indeed, in Mo_6S_8, the separation between the two S^i atoms is large in comparison to twice ionic radii of S. This feature explains the poor stability of this binary sulfide that cannot be obtained by direct solid-state routes at high temperature in contrast to the selenium and tellurium homologs, Mo_6Se_8 and Mo_6Te_8. It can however be obtained in soft conditions by deintercalation of $A_xMo_6S_8$ ternary sulfides.[44] The "Mo_6S_8" framework can also be stabilized by the replacement of the two S^i atoms belonging to the two fc-clusters by two Br^i atoms leading to $Mo_6S_6Br_2$ which is prepared in a manner similar to that of Mo_6Se_8 or Mo_6Te_8.[8] Indeed, the stabilization of the $Mo_6S_6Br_2$ structure is related to the short Br^i-Br^i interatomic distance that corresponds to the sum of ionic radii.

$A_xMo_6L_8$ Ternary Compounds. The difference between the $A_xMo_6L_8$ and Mo_6L_8 series is the occupation of the octahedral cavity by A the cation. For further relevant comparisons with the $A_nM_6L_{12}(Z)$ series, among the numerous examples of ternary $A_xMo_6L_8$ compounds, we will only consider those obtained with the large Pb^{2+} cation and with the smallest Cu^+ cation. In all of these compounds, the L^i ligands from the fc-clusters are always involved in the coordination sphere of the cations. In $PbMo_6S_8$ or $PbMo_6Se_8$, the position of the Pb^{2+} cation merges with that of the O centroid.[17] The Pb-L^{i-a} distances are close to the O−L^{i-a} ones (O, centroid of the octahedral cavity) in the corresponding Mo_6L_8 binary chalcogenides, but the Pb−L^i distance is larger than the O−X^i ones. This results in an elongation of the *c* parameter while *a* remains unchanged. Note that "$PbMo_6Te_8$" has not been reported probably because the presence of Pb on the O centroid would distort the $Mo_6Te^i{}_2Te^{i-a}{}_{6/2}Te^{a-i}{}_{6/2}$ framework too much along the *c* axis. In $Cu_{1.38}Mo_6S_8$, the copper is shifted from the O centroid position.[47] Indeed, the localization of Cu^+ on the O centroid would induce unrealistic Cu−S interatomic distances. The shift from the O position toward the edges of the c-cluster octahedron enables the stabilization of the copper cation in the tetrahedral sites of sulfur that correspond to two independent crystallographic positions: Cu1 (coordination, two S^i from the fc-clusters and two S^{i-a} from the c-clusters) and Cu2 (coordination, one S^i from the fc-clusters and three S^{i-a} from the c-clusters). This shift of the copper from the O position induces a distortion of the octahedral cavity leading to a S^i-S^i interatomic distance of 4.126 Å, which is shorter than that found in Mo_6S_8 (4.703 Å). Finally, the ability of the $M_6S^i{}_2S^{i-a}{}_{6/2}S^{a-i}{}_{6/2}$ (or Se) skeleton to be reduced in a reversible way (variation of the VEC) combined with its elasticity versus the replacement of large divalent cations

(44) Chevrel, R.; Sergent, M.; Prigent, J. *Mater. Res. Bull.* **1979**, *9*, 1487.
(45) Bars, O.; Guillevic, J.; Grandjean, D. *J. Solid State Chem.* **1973**, *6*, 48.
(46) Miller, G. J.; Smith, M. *Acta Crystallogr. C* **1998**, *54*, 709.
(47) Yvon, K.; Paoli, A.; Fluekiger, R.; Chevrel, R. *J. Solid State Chem.* **1993**, *102*, 54.

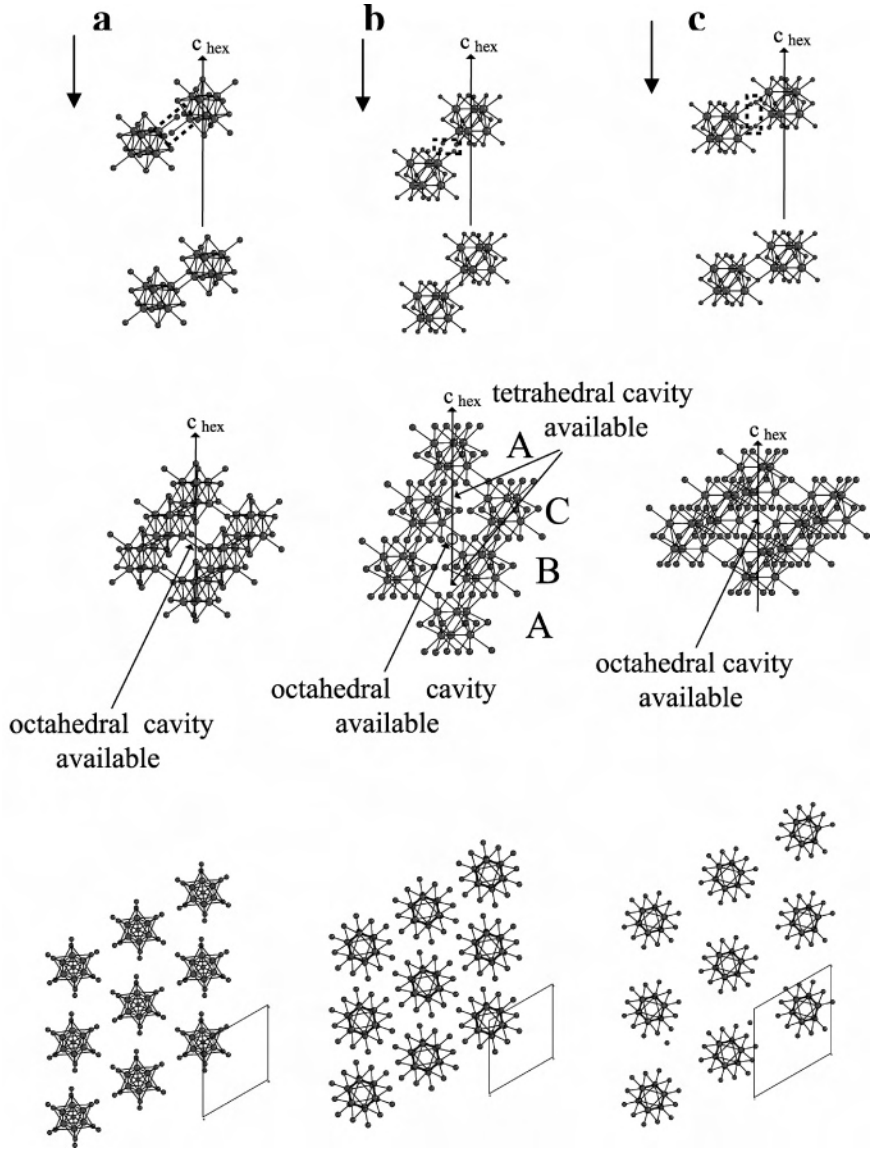

Figure 8. Representation of the condensation of M_6L_{14} and M_6L_{18} units via isotropic inner−apical and apical−inner bridges. On a same column, projection of the structure along [1 0 0], projection of a cluster layer along [0 0 1] with its bonded ligands: (a) Chevrel Phase, (b) $CsEr_6I_{12}C$ and $Na_{0.66}(Sc_{1.33}Nb_{0.66})Nb_6O_{12}$, and (c) $NaLa_6I_{12}Os$.

by smaller monovalent cations explain the interesting intercalation properties of Chevrel Phases. One can conclude that the $Mo_6S_2{}^iS^{i-a}{}_{6/2}S^{a-i}{}_{6/2}$ framework is stabilized by the occupation of the octahedral O cavity, while no cation can occupy the tetrahedral cavity.

$A_nM_6L_{12}(Z)$ Series: $CsEr_6I_{12}C$ and $NaLa_6I_{12}Os$. As observed in Chevrel Phases, the $A_nM_6L_{12}(Z)$ series are based on octahedral clusters centered at the apexes of a rhombohedral unit cell (Figure 8b and c). $CsEr_6I_{12}C$[42] and $NaLa_6I_{12}Os$[43] have been chosen among the members of the $A_nM_6L_{12}(Z)$ series as relevant examples for the discussion of unit condensation and cationic site sizes. First, these two compounds are both based on $M_6L_{18}(Z)$ units sharing inner−apical ligands in the three directions of the space with a same developed formula $M_6L_6{}^iL^{i-a}{}_{6/2}L^{a-i}{}_{6/2}(Z)$. Another similarity is a cubic close packing of units with an ABCA sequence leading to octahedral and tetrahedral cavities. However, their structures differ from each other by two different condensation mechanisms between adjacent $M_6L_{18}(Z)$ units in the rhombohedral unit cell represented in Figure 8b and c. In Chevrel Phases, the geometry of the Mo_6L_{14} unit and its disposition along the 3-fold axis make only one mechanism of condensation via isotropic inner−apical bridges between one unit and six adjacent ones (three below and three above) (Figure 8a) possible. As it can be seen in Figure 9, the condensation of units through three inner−apical bridges cannot involve the inner ligand located on the 3-fold axis of the rhombohedral unit cell. On the other hand, the $M_6L_{18}(Z)$ unit offers two possibilities for such inner−apical connections (Figure 8b and c). Indeed, in $NaLa_6I_{12}Os$ (Figure 8c), the inner−apical connections involve the inner ligands from the equatorial plane of the M_6L_{18} units, while in $CsEr_6I_{12}C$ (Figure 8 b), the inner−apical connections involve the external inner ligands of the units. This results in interpenetrated layers in $NaLa_6I_{12}Os$ with a *c*/*a* ratio of 0.72, while the *c*/*a* ratio is 1.85 in $CsEr_6I_{12}C$. Consequently, in the latter iodide, the units are compacted within the layers according

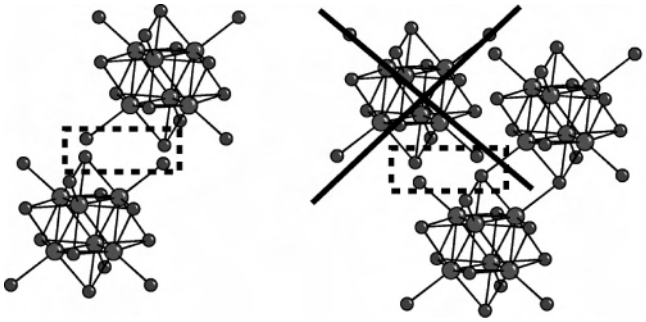

Figure 9. Condensation of units through three inner−apical brigdes cannot involve the inner ligand located on the 3-fold axis of the rhombohedral unit cell.

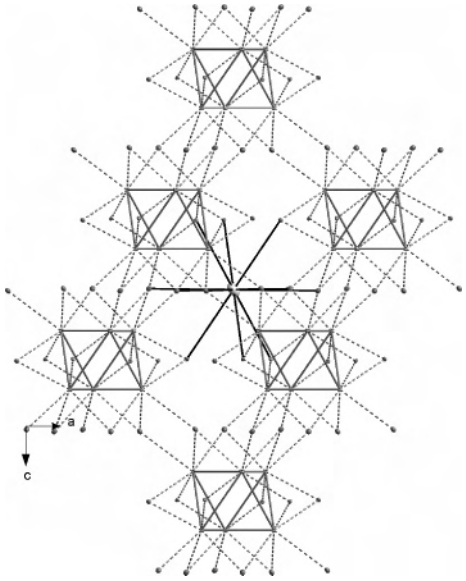

Figure 10. Representation of the environment of Cs in $CsEr_6I_{12}C$.

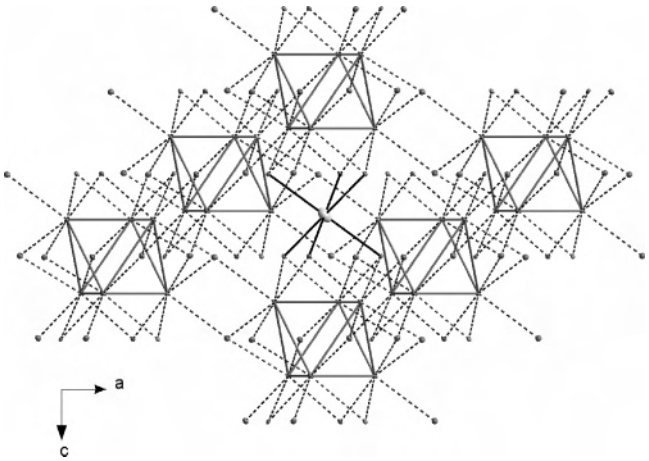

Figure 11. Representation of the environment of Na in $NaLa_6I_{12}Os$.

a "hard-sphere" model but not in $NaLa_6I_{12}Os$ for which the successive layers are embedded in each other (Figure 8c).

The positions of Cs and Na merge with that of the O centroid in $CsEr_6I_{12}C$ and $NaLa_6I_{12}Os$, respectively (Figures 10 and 11). However, because of the two different mechanisms of condensation discussed above, their coordination spheres for the ligands are completely different. Cs lies in a ligand site built up from twelve ligands belonging to the c-clusters. On the other hand, Na lies in a regular site of ligands built up from inner ligands belonging to two fc-clusters. Similar to what has been observed in Chevrel Phase, the T centroid is sandwiched between a M_3 triangle and inner ligands with $T-X^i$ and T−M distances that prevent the localization of additional cations, even small ones, in the tetrahedral cavity in $NaLa_6I_{12}Os$. On the other hand, in $CsEr_6I_{12}C$, the T centroid is surrounded by three inner ligands belonging to a same unit and to three inner−apical ligands belonging to three other units. Moreover, the T−I distances are compatible with an additional small countercation in the tetrahedral cavities. From the topological point of view, it turns out that the structure of $NaLa_6I_{12}Os$ is more closely related to that of the Chevrel Phase than that of $CsEr_6I_{12}C$ to which $Ti_2Nb_6O_{12}$ and $Na_{0.66}(Sc_{1.33}Nb_{0.66})Nb_6O_{12}$ are related.

$A_nBNb_6L_{12}$(Z) Series: $Ti_2Nb_6O_{12}$ and $Na_{0.666}(Sc_{1.33}Nb_{0.66})Nb_6O_{12}$. As stressed in the preceding section, the structures of $Ti_2Nb_6O_{12}$ and $Na_{0.666}(Sc_{1.33}Nb_{0.66})Nb_6O_{12}$ are related to that of $CsEr_6I_{12}C$. The inner−apical connections are achieved via the inner external ligands of the clusters that enable the occupation of the tetrahedral cavity in the oxides by small countercations, such as titanium $Ti_2Nb_6O_{12}$ or niobium and scandium in $Na_{0.66}(Sc_{1.33}Nb_{0.66})Nb_6O_{12}$. In $Ti_2Nb_6O_{12}$, the octahedral cavity is empty, while it is occupied by Na^+ in $Na_{0.66}(Sc_{1.33}Nb_{0.66})Nb_6O_{12}$. Because of its large size, the position of Cs^+ in $CsEr_6I_{12}C$ merges with that of the O centroid in manner similar to that of Pb^{2+} in Chevrel Phases. On the other hand, the small size of Na^+ compared to that of Cs^+ induces a shift from the O centroid within the octahedral cavity. This shift of Na toward the edges of the octahedron of the c-clusters is comparable to the shift of Cu1 in $Cu_xMo_6S_8$ (see above). Because of a similar topology of the cluster frameworks between the members of the A_x-Mo_6S_8 series and $Na_{0.66}(Sc_{1.33}Nb_{0.66})Nb_6O_{12}$, as well as the occupation of the octahedral cavity in both compounds, one could suspect the presence of intercalation properties in the title oxide. Several attempts have been made to deintercalate Na from $Na_2(Sc_4Nb_2)(Nb_6O_{12})_3$ either by direct solid-state reaction with I_2 or in refluxing acetonitrile as previously successfully performed with the $Na_xMo_6L_8$ (L = S and Se) series.[48] From the electronic point of view, such a deintercalation should have been successful since it corresponds to the loss of less than one electron from the Nb−Nb bonding states (14 to 13.33). Moreover, a niobium cluster compound has already been reported with a VEC of $13e^-/Nb_6$ (KNb_8O_{14}[27]). A closer look at the structure and, in particular, at the second neighboring ligands of sodium has shown that this cation is imprisoned in a cage of ligands in which the O−O distances vary from 2.952 to 3.559 Å. In Chevrel Phases, the disposition of the octahedral cavity allows the formation of channels from which cations can be easily deintercalated. This difference can be attributed to the steric hindrance of the 12 inner ligands in the M_6L_{18} units compared to that of the 8 inner ligands in the M_6L_{14} ones, as well as to a different mode of condensation as discussed above.

(48) Tarascon, J. M.; Hull, G. W.; Marsh, P.; Haar, T. *J. Solid State Chem.* **1987**, *66*, 204.

Concluding Remarks

To conclude, despite similar topologies between the Chevrel Phase and $A_nBNb_6O_{12}$ series, intercalation properties are not expected in the niobium oxides. LMTO calculations suggest that for the Nb_6O_{12} framework the optimun VEC value is 14 and that reduction cannot be achieved. A semiconducting behavior is therefore expected as previously measured in $Ti_2Nb_6O_{12}$. Metallic properties could be obtained for VEC ranging from 13 to 14 e^-/Nb_6, but such oxides could be obtained only by direct solid-state synthesis and not by a deintercalation process.

Acknowledgment. The Centre de Diffractométrie de l'Université de Rennes 1 is acknowledged for the data collection on the Nonius KappaCCD X-ray diffractometer. In particular, we greatly thank the useful advice of Dr. T. Roisnel. We are also indebted to M. Bohn (IFREMER, Brest) for his assistance with the EPMA studies. S.C. and C.P. are grateful to "Fondation Langlois" for its financial support. B.F., R.G., and J.-F.H. thank the Pôle de Calcul Intensif de l'Ouest (PCIO), the Institut de Développement et de Ressources en Informatique Scientifique (IDRIS-CNRS), and the Centre Informatique National de l'Enseignement Supérieur (CINES) for the use of their computing facilities.

Supporting Information Available: An X-ray crystallographic file of $Na_2(Sc_4Nb_2)(Nb_6O_{12})_3$, in CIF format is available This material is available free of charge via the Internet at http://pubs.acs.org.

IC0512678